Nano-Structures & Nano-Objects 46 (2026) 101676

Contents lists available at ScienceDirect

Nano-Structures & Nano-Objects

journal homepage: www.elsevier.com/locate/nanoso

Electronic and spectral characteristics of pyrrole adsorption on $Al_{12}N_{12}$ and $Al_{12}P_{12}$ nanocages: A DFT-based sensing assessment

Jamelah S. Al-Otaibi [a], Y.Sheena Mary [b], Unnati Jethawa [c], Brahmananda Chakraborty [d,e], Maria Cristina Gamberini [f,*]

[a] Department of Chemistry, College of Science, Princess Nourah Bint Abdulrahman University, P.O. Box 84428, Riyadh 11671, Saudi Arabia
[b] Department of Physics, FMN College (Autonomous), Kollam, University of Kerala, Kerala, India
[c] Department of Physics, SIES College of Arts, Science & Commerce, Mumbai, Maharashtra 400022, India
[d] High Pressure & Synchroton Radiation Physics Division, Bhabha Atomic Research Centre, Trombay, Mumbai, Maharashtra 400085, India
[e] Homi J Bhabha National Institute, Bhabha Atomic Research Centre, Trombay, Mumbai, Maharashtra 400085, India
[f] Department of Life Sciences, University of Modena and Reggio Emilia, via G. Campi 103, Modena 41125, Italy

ARTICLE INFO

Keywords:
DFT
Pyrroles
RDG
Nanocages

ABSTRACT

This work presents a comprehensive Density Functional Theory (DFT) investigation of the adsorption behavior of two pyrrole derivatives (PYI and PYII) on $Al_{12}N_{12}$ and $Al_{12}P_{12}$ fullerene-like nanocages, aiming to evaluate their suitability for sensing and drug-delivery applications. Geometry optimization, adsorption energy calculations, electronic structure analysis, molecular descriptors, and solvent effects were examined using the wB97XD/SDD level of theory. Both PYI and PYII exhibit spontaneous, exothermic, and chemisorptive binding onto the nanocages, with the presence of a strong adsorption observed for PYII and for $Al_{12}P_{12}$, particularly in aqueous media. Adsorption induces pronounced charge distribution, reduction of HOMO-LUMO gaps, increase in dipole moment and polarizability, and significant modulation of frontier orbital distribution, all indicating enhanced electronic reactivity and stronger surface interactions. UV-Vis and Raman analyses further reveal marked red shifts, reduced absorption intensities, and surface-enhanced Raman scattering (SERS)-active vibrational enhancements, confirming strong coupling between the pyrroles and the nanocages. Natural Bond Orbital (NBO) and Reduced Density Gradient (RDG) analyses highlight dominant hyperconjugative interactions and mixed attractive/van der Waals contributions stabilizing the adsorbed complexes. Molecular docking with acetylcholinesterase (1EVE) demonstrates substantially improved binding affinities for the adsorbed systems compared to the isolated pyrroles, suggesting potential for targeted therapeutic delivery. Collectively, these findings, identify Al-based nanocages as promising candidates for pyrrole sensing, photocatalytic enhancement, and drug-carrier applications.

1. Introduction

Due to their applications in wide sectors, including bioelectronics, biomedicine, shielding technologies and display materials conducting polymers (CPs) had been recently attracted increasing attention [1–7]. Their special mechanical and electrical qualities-such as their high mobility, excellent stability, optical clarity, low processing temperature have sparked interest [8,9]. These materials' conducting nature results from the delocalized pi-electrons, which offer an easy avenue for electron mobility. Because of its non-toxicity, high conductivity, band gap and ease of synthesis, polypyrrole is one of the most thoroughly investigated CPs [10]. The photo catalyst PY has been specifically employed for the purpose of removing and degrading environment contaminants due to its exceptional redox, ion exchange, and cost-effectiveness [11]. Environmental factors can cause PY to lose some of its electrical conductivity, which limits its use in a variety of applications [12]. Consequently, increasing its adsorption efficiency is required. Adding nanostructures to polymers is one of the promising ways to get around this problem and increase the surface area of PY. This makes polymers a better adsorbent for the photo-catalytic degradation of different pollutants and medications [12]. Because of their special physical characteristics, nano materials can be used as dopants to

* Corresponding author.
E-mail address: mariacristina.gamberini@unimore.it (M.C. Gamberini).

https://doi.org/10.1016/j.nanoso.2026.101676
Received 15 December 2025; Received in revised form 23 January 2026; Accepted 29 April 2026
Available online 12 May 2026

improve the conductivity of polymers. They can also increase the adsorption capacity, solubility, and hydrophobicity of the polymers, which can results an increased potential photo-catalytic activity [13,14]. The ability to absorb the greatest number of photons and as an effective catalyst is characteristics of appropriate nanomaterials for photo catalytic applications. Because of this, a semiconductor needed for photo catalytic applications needs to have a band gap between 1.8 and 2.2 eV [15,16]. Ti_2O or ZnO are used as coating materials to PY to increase its conductivity and crystalline nature [17]. Furthermore, it has been claimed that several strategies, including composites, and band gap minimization, improve PY performance [18].

The $Al_{12}N_{12}$ and $Al_{12}P_{12}$ fullerene-like nanocages were chosen for this study because of their special combination of strong interaction potential with molecular adsorbates, tunable electronic properties, and structural stability, which makes them especially appealing for biomedical and sensing applications. Previous theoretical studies have demonstrated that Al-based nanocages frequently display stronger adsorption properties in comparison to analogous boron-based cages; for instance $Al_{12}N_{12}$ has been found to adsorb different gas molecules strongly than $B_{12}N_{12}$, indicating increased reactivity and sensitivity potential [19]. Phosphorus incorporation tends to decrease the HOMO-LUMO gap and increase polarizability, which can improve electronic response upon adsorption, as demonstrated in $Al_{12}P_{12}$ in comparison to other group III-V cages, according to comparative studies across heteronuclear $X_{12}Y_{12}$ nanocages [20]. Additonally, recent DFT research has shown significant electronic perturbations and efficient chemisorption for medication and pollutant molecules on Al-containing cages, underscoring their potential in sensing and delivery contexts [21]. While other nanocages like $B_{12}N_{12}$ or $Be_{12}O_{12}$ have been investigated for gas sensing and adsorption, $Al_{12}N_{12}$ and $Al_{12}P_{12}$ are particularly good candidates for the systems under study due to their unique combination of stronger adsorption energetics, favorable electronic modulation, and potential for significant spectroscopic response. Notably, the current work expands on this well-established framework to investigate adsorption, electrical, and spectroscopic signals pertinent to pyrrole derivatives, offering a targeted but widely applicable contribution to the design of nanocage-based sensors and carriers.

The findings demonstrate that metal-doped $B_{12}N_{12}$ nanoclusters have substantial affinity for β-lapachone and tunable electronic structures, highlighting their potential as stable and effective nanocarriers for drug administration and related biological applications [22]. Identification of Fe- and Mn-doped systems as viable possibilities for sensitive and quick detection of the drug penicillamine, especially under biologically relevant solvent conditions, and provided a theoretical basis for developing effective $Si_{12}C_{12}$-based metal-doped nanocage sensors [23]. Through DFT calculations, it was reported that Ga_n, $Be_{12}O_{12}$ and $GaBe_{11}O_{12}$ clusters show strong to moderate chemisorption and high sensitivity toward phenytoin; Ga_3 and $GaBe_{12}O_{12}$ emerge as particularly promising regeneragable nanosensors because of their short recovery times in aqueous environments [24]. The crucial significance of metal doping in adjusting cluster reactivity and sensing performance was highlighted by Derdare et al.,'s DFT calculations, which showed that both pure and metal-doped C_{20} clusters (Ru, Ir, and Au) exhibit strong and selective adsorption toward NO_2, N_2O_2, and NH_3 molecules [25]. The results demonstrate that $B_{12}N_{12}$ nanocages doped with Cu and Rh have significantly improved gas sensing and catalytic performance, facilitating effective NO detection by chemisorption and encouraging H_2S dissociation via strong surface-adsorbate interactions [26]. The adsorption behavior of neural and zwitterionic serine on pristine and Pt-decorated $B_{12}N_{12}$ fullerenes is clarified in literatue. Amine-driven chemisorption on Pt-$B_{12}N_{12}$ is found to be the most stable interaction, and adsorption-induced band-gap changes pertinent to biomolecular applications are highlighted [27]. MC_{23} clusters, especially those containing Mn, Ru, Rh, and Pd, have low energy barriers and easy O_2 desorption, which makes them highly active and regenerable nanocatalysts for effective N_2O breakdown [28].

These days, the pharmaceutical industry relies heavily on nanotechnology to treat cancer and other diseases with targeted medicines [29,30]. One of the most difficult issues in treatment of cancer is the use of nano structures for medicine delivery to the impacted bodily sections. Additionally, the therapy of intracellular disorders has greatly advanced because to nano structured medicinal carriers. Due to their improved surface/volume ratio over conventional micro sensors, researches are focussing on the properties of nanomaterials as sensors [31,32]. Many nanostructures, including cages, fullerene, carbon nanotubes, and variants of graphene, have been extensively documented for use in biological, drug delivery, bio-sensing, cell targeting and bio-imaging [33,34]. Because of their remarkable mechanical and electrical qualities as well as their extraordinary chemical stabilities, inorganic boron and aluminum nitride nanosheets, chains, cones, clusters and nanotubes have garnered a lot of attention recently [35–37]. Previous investigations on various $(XY)_{12}$ (X = B, Al,… and Y═N,P…) revealed that the most stable structure is an $X_{12}Y_{12}$ fullerene like nanocluster [38,39]. The study and publication of the energy and structure of AlN nanoclusters showed that AlN is the most thermodynamically stable one [40].

A recent study provides essential insights for the logical design of next generation N_2 sensors and metal-free catalytic platforms for sustainable nitrogen fixation by elucidating a strong, polarization-driven mechanism for N_2 activation and conversion to the NH_3 on $B_{12}N_{12}$ in aquatic conditions [41]. By showing how their tunable electronic structure and varied adsorption interactions with DNA nucleobases enable improved sensitivity, stability, solubility, and charge-transport properties necessary for effective biosensors and drug delivery systems, boron nitride fullerenes are important in biomedical and sensing applications [42]. In order to address a crucial issue in the remediation of pharmaceutical pollution, a molecular-level theoretical framework is presented to demonstrate how metal-encapsulated $Al_{12}N_{12}$ nanocages can be logically engineered to improve the adsorption and controlled removal of fluoroquinolone antibiotics from aqueous environments [43].

Heteroatom engineering and doping techniques have become effective methods in recent years for adjusting the structural, electrical, and sensing characteristics of nanomaterials in a variety of applications. For instance, due to the formation of active sites and altered electronic structure, heteroatom-doped graphene and related carbon nanoarchitectures have shown improved adsorption, charge transfer, and sensitivity toward a variety of analytes, highlighting the importance of dopant selection in sensor design [44]. Similarly, first-principles research on phosphide nanocages, such as $Al_{12}P_{12}$, has demonstrated their promise as efficient sensing platforms for volatile organic chemicals with notable adsorption energies and electronic perturbations upon binding, exceeding their $Al_{12}N_{12}$ counterparts [45]. These results imply that heteroatom incorporation and structural modulation can improve interaction strength, electronic response, and biological affinity in both 0D and 2D nanostructures, which may explain the superior performance of $Al_{12}P_{12}$ seen in this study. Specifically, customized 2D materials and nanocages have been studied more and more for biosensing and biomedical applications, where sensitivity, selectivity, and biocompatibility are maximized through heteroatom doping and surface functionalization [46]. These more general examples from literature highlight that heteroatom and structural tuning represent a promising design paradigm for the development of next generation aluminum-based and related nanomaterials for sensing and biomedical applications, and they encourage future system-specific studies to validate and extend these trends, even though the current work focuses on comparing $Al_{12}N_{12}$ and $Al_{12}P_{12}$ as prototypical systems. In order to determine whether $Al_{12}N_{12}$ and $Al_{12}P_{12}$ nanocages are appropriate for use in the adsorption and detection of PYs, the current work attempts to investigate the interaction and adsorption behavior of these nanocages toward the drug. Also to research the adsorption and sensitivity, DFT techniques were used to investigate various characteristics as well as binding energies.

2. Methods

The DFT calculations were performed with Gaussian16 and Gaussview programs [47,48]. With the SDD basis set, wB97XD was employed in the investigation [49]. Drug-nanocage complexes and adsorption phenomena are examples of systems where noncovalent interactions, dispersion forces, charge transfer, and polarization effects are significant. The wB97XD functional is a range separated hybrid functional with built-in long range dispersion corrections. As evidenced by recent work on nanosheet-drug systems and adsorption studies using wB97XD to accurately describe noncovalent binding, this functional has been widely used in studies of molecular adsorption and drug-material interactions. It is known for its reliability in capturing dispersion and long range charge transfer with reasonable computational cost [50]. Although quantitative accuracy can be further validated by benchmarking against higher level methods or additionally hybrid/meta hybrid functional (e.g., M06 2X, CAM B3LYP), such comparisons are frequently computationally prohibitive for large complexes and are not anticipated to alter the qualitative trends observed in binding affinities and interaction characteristics. In order to accurately describe noncovalent interactions, long-range transfer, and π-π interactions – all of which are essential to nanocage-pyrrole adsorption systems – the wB97XD functional was chosen. For systems where dispersion and electronic delocalization are important, long-range corrected functional like wB97XD have been demonstrated to perform better than traditional hybrid functionals, especially in adsorption and surface-molecule interaction studies [51–53]. The SDD basis set maintains consistent accuracy for computations of electronic structure and adsorption energy while utilizing effective core potentials to treat larger atoms in a balanced and computationally efficient manner. Numerous investigations using nanoclusters and adsorption processes have effectively used this basis set [54,55]. While B3LYP-D3 is a well-known functional for dispersion-corrected calculations, wB97XD is particularly useful for predicting adsorption energies, frontier molecular orbitals, and charge-transfer characteristics in extended nanostructures because it naturally includes long-range correction in addition to dispersion effects. For dispersion-dominated and long-range interaction systems, comparative benchmarks have demonstrated that wB97XD produces findings more in line with advanced techniques [52,53].

Every complex under study was optimized without any limitations. For each system, a single initial geometric interaction configuration was considered, in which the drug molecule was placed parallel to the nanocage surface with a separation less than 3 Å for maximum interaction and subsequently fully optimized to locate the minimum-energy complex In order to verify the minima structure for every geometric, frequency calculations were carried out and the structures were energetically minima. This concept was successfully applied in earlier research to explain the electrical characteristics and interactions of drugs and bio-molecules with these kinds of nanocages [56,57]. $E_{bind} = E_{complex} - E_{PY} - E_{nanocage}$ is the formula used to compute the binding energy of each complex, where $E_{complex}$, E_{PY}, and $E_{nanocge}$ is total energies of complexes, PY and nanocages. The complexes are simulated at geometric gCP, which can treat both inter- and intra-molecular BSSE [58]. The wB97XD-gCP-D3/SDD energy corrections are also made from Gimme's web service [59–61]. Binding energies in aqueous phase were determined via the application of solvent model density (SMD) [62]. Aqueous-phase adsorption energies were calculated using the SMD continuum solvation model, which efficiently accounts for bulk solvent effects while providing reliable trends in binding energetics. Every analyzed compound's quantum molecular characteristics were examined [63,64]. The RDG isosurfaces and scatter plots were drawn using Multiwfn [65] and VMD [66] software.

3. Results

3.1. Adsorption and chemical properties

Figures 1 and S1 displays geometries, FMOs and MEP plots of PYI, PYII and AlN and AlP nanocages. The optimized geometries of AlN-PYI, AlP-PYI, AlN-PYII and AlP-PYII are shown in Fig. 2. Fig. 1c show that there is a positive zone in the H atoms, particularly for the NH group and a significant negative density region along the ring of PYI and PYII (red and yellow). An intermediate negative electron density zone can be seen along the AlN/P, based on MEP plots (Figure S1c). When the nanocages are optimized in the aqueous phase, no appreciable alterations take place.

In complex AlN-PYI the interactions with PYI through the C28/29, N25 and H33 atoms of PYI, with Al7-C28/29 = 2.33/2.93, N21-C28 = 3.54, Al7-N25 = 3.43, N9-C28 = 3.28 Å and Al7-H33 while in AlP-PYI, the interaction is through C28, C26, H33 and H31, with Al9-C28/26 = 2.41/2.81, Al9-H33/31 = 2.64/3.19 Å. For AlN-PYII the interaction is through C33, N38, H40, H43 with Al7-N38 = 2.12, Al7-H40 = 2.52, Al7-C33 = 3.08, N9-H30 = 1.86, Al4-H30 = 3.10, Al7-H43 = 3.02 and N9-H40 = 3.19 Å while in AlP-PYII, the interaction is through C26, N25, H31, H30, and H40 with Al11-C26 = 2.18, Al11-H31 = 2.63, Al11-H30 = 3.09, Al11-N25 = 2.90 and P23-H40 = 3.08 Å. The adsorption energies (BSSE corrected) are in vacuum/water phases are −25.62, −27.19 (-23.98, −25.23)/-33.94, −36.17 (-32.22, −35.64) kcal mol^{-1} for PYI and −32.07, −34.03(-31.73, −33.19)/-38.94, −39.42 (-37.38, −38.85) kcal mol^{-1} for PYII with AlN and AlP nanocages, respectively. Highest energy is found to with AlP adsorption and is also it increases in the solvent phase (Table 1). The drugs always take on an oblique orientation in relation to the cages during adsorption (Fig. 2) [67].

In PYI, both FMOs are over PYI, except NH in HOMO and for PYII, FMOs (Fig. 1b) are distributed on entire regions, except for H atoms in HOMO and LUMO; also there is no LUMO concentration on CH as in Fig. 1b. The distribution of FMOs was roughly distributed on eletcronegative, N, P and electropositive, Al (Figure S1) [68].

In AlN-PYI/PYII, HOMO is over drugs while LUMO is over the cages (Fig. 3a and c). In AlP-PYI, both FMOs are in the cage (Fig. 3b) and in AlP-PYII, HOMO is over the cage and LUMO is over PYII. The redistribution of electron densities suggests charge transfer in all systems during adsorption [69].

The HOMO/LUMO energies of AlN, AlP, PYI and PYII are −6.47, −6.82, −5.58, −4.66/-2.54, −3.432, −1.27, −0.16 eV (Table 2). The Fermi level energies for AlN/P, and PYI/ PYII are −4.51/-5.12 and −3.42/-2.41 eV. The Eg for AlN/P, PYI/PYII are 3.93/3.39 and 4.31/4.51 eV, suggesting that AlP has highly conductive than AlN. The Eg values may also be used to study the kinetic stability of nanocages. AlP was therefore more reactive than AlN due its poorer kinetic consistency. In both the vacuum and water phases, the band gap for all compounds reduces upon adsorption when compared to their pristine values. The hardness exhibits the same band gap variation trend. The electrophilicity values of PYI and PYII increases after adsorption with nanocages revealing the biological activity (Table 2) [70].

Fig. 4 shows the Molecular Electrostatic Potential (MEP) maps of all adsorbed complexes in which there is modification for the reactive zones in comparison with that of pristine ones, which indicate charge transfer within the components [71,72]. The DOS spectra of PY systems clearly give new energy levels after adsorption (Figures S2 and S3).

The values of DM of nanocages are nearly zero while that of PYI and PYII are 1.90 and 2.60 Debye. After adsorption dipole moment rises and high for adsorption with AlP both in vacuum and aqueous media (Table 1). The dipole moments are 6.89 and 8.26 for PYI and 4.35 and 10.47 for PYII when they interact with AlN and AlP cages. The polarizability of all adsorbed complexes are high in comparison with that of pristine values (Table 1) which produces increase in Raman intensity for different modes in the complexes due to SERS enhancement [73,74].

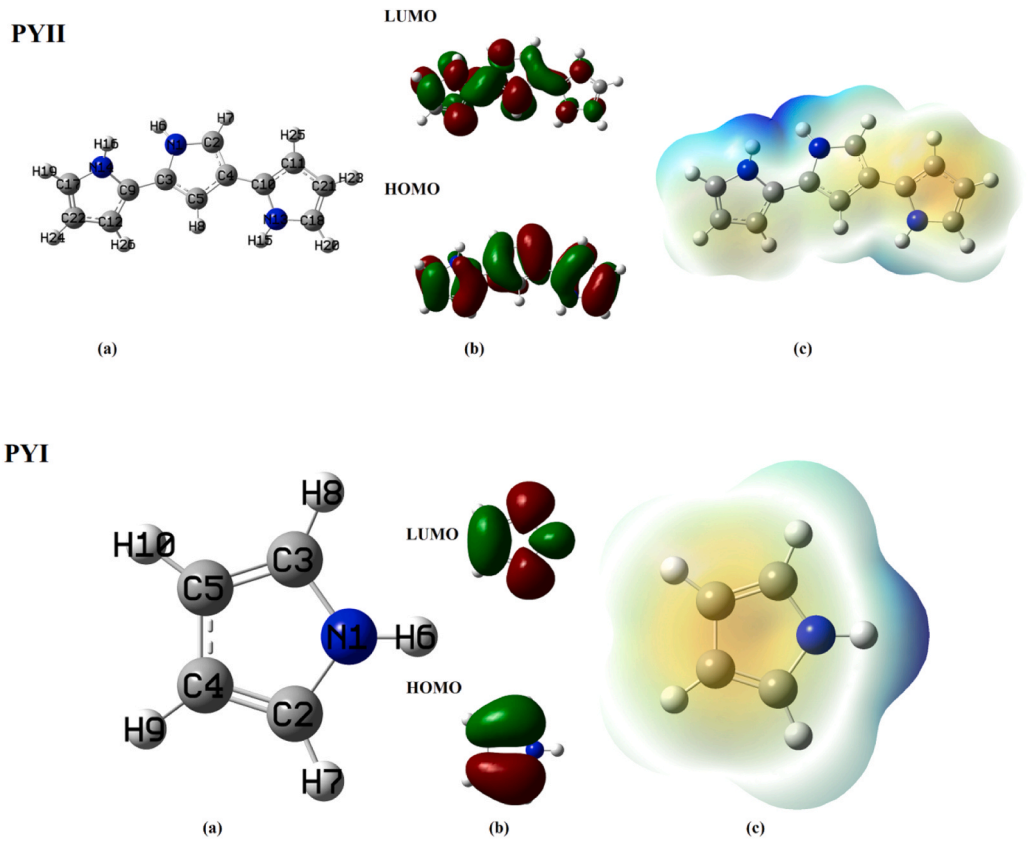

Fig. 1. PY's (a) optimized geometry, (b) FMOs (c) MEP plots.

Table 1
Energies, dipole moments, polarizability and adsorption energies.

Systems	Energy (Hartree)	Dipole moments (Debye)	Polarizability (A.u)	Adsorption energy (kcal mol^{-1})	E_{gCP}-D3 (kcal mol^{-1})
PYI	-210.11	1.90	39.68	-	-
PYII	-627.97	2.60	144.73	-	-
AlN	-3567.24	0.01	287.85	-	-
AlP	-7006.80	0.00	613.56	-	-
Vacuum					
AlN-PYI	-3777.40	6.89	336.42	-25.62	-23.98
AlP-PYI	-7216.96	8.26	639.61	-27.19	-25.23
AlN-PYII	-4195.26	4.35	456.21	-32.07	-31.73
AlP-PYII	-7636.82	10.47	775.22	-34.03	-33.19
Water					
AlN-PYI	-3777.41	8.32	504.14	-33.94	-32.22
AlP-PYI	-7216.97	10.61	416.28	-36.17	-35.64
AlN-PYII	-4195.27	5.69	655.00	-38.94	-37.38
AlP-PYII	-7636.83	13.07	479.82	-39.42	-38.85

Significant variations in contact strength and spontaneity are revealed by the computed thermodynamic parameters for the adsorption of PYI and PYII on AlN and AlP nanocages. Stronger binding to both nanocages is indicated by PYII's much higher adsorption energies in vacuum as opposed to PYI. AlP consistently exhibits somewhat higher binding energies than AlN among the two nanocages, especially for PYII, where ΔG reaches −177.50 $kcalmol^{-1}$ indicating that phosphide-based cage offers more advantageous adsorption (Table 3). Adsorption energies for both PYI and PYII continue to rise in aqueous conditions, indicating improved interactions in the presence of solvent. Significantly, PYII complexes exhibit stronger negative entropy shifts (ΔS), particularly in water (-54.62 kcal mol^{-1} K for AlN-PYII), suggesting a greater degree of structural ordering upon adsorption. AlP nanocages exhibit better stability in both vacuum and aqueous settings, and overall, PYII exhibits stronger, more spontaneous adsorption than PYI. This highlights the impact of both molecular structure and nanocage composition on thermodynamic favourability.Table 3

In the current study, the calculated adsorption energies for pyrrole on nanocages in the liquid phase (ranging from −33.94 to −39.42 kcal mol^{-1}) suggest the presence of a strong interactions that are often classified as chemisorption in DFT-based investigations (typical chemisorption energies span similar magnitudes when compared with nanomaterial–drug systems in recent literature) [75]. Strong adsorption energies can enhance the stability of drug–carrier complexes, ensuring that the payload remains associated with the delivery vehicle during circulation in physiological environments, which is especially relevant given the dynamic nature of solvent and biomolecule interactions in biological fluids [76]. Moreover, recent reviews underscore that tailored surface interactions, including the presence of a strong binding at select active sites, can be advantageous for maintaining drug integrity and preventing premature release prior to reaching target tissues [75]. However, in the context of a drug delivery system, excessively the presence of strong binding at all available surface sites could theoretically reduce the capacity for additional payload loading or hinder controlled release. It is therefore important to contextualize these adsorption energies with respect to environmental triggers (e.g., pH, ionic strength) that modulate binding strength under physiological conditions. Stimuli-responsive release strategies exploit variations in the local biological milieu-such as lower pH in tumor microenvironments-which have been demonstrated in mesoporous and functionalized nanoparticle systems to weaken adsorption sufficiently to facilitate drug release while preserving the presence of a strong binding during systemic transport [77]. This balance between adsorption strength for transport stability and controlled release in targeted environments must be carefully considered when evaluating nanocage performance for biomedical applications.

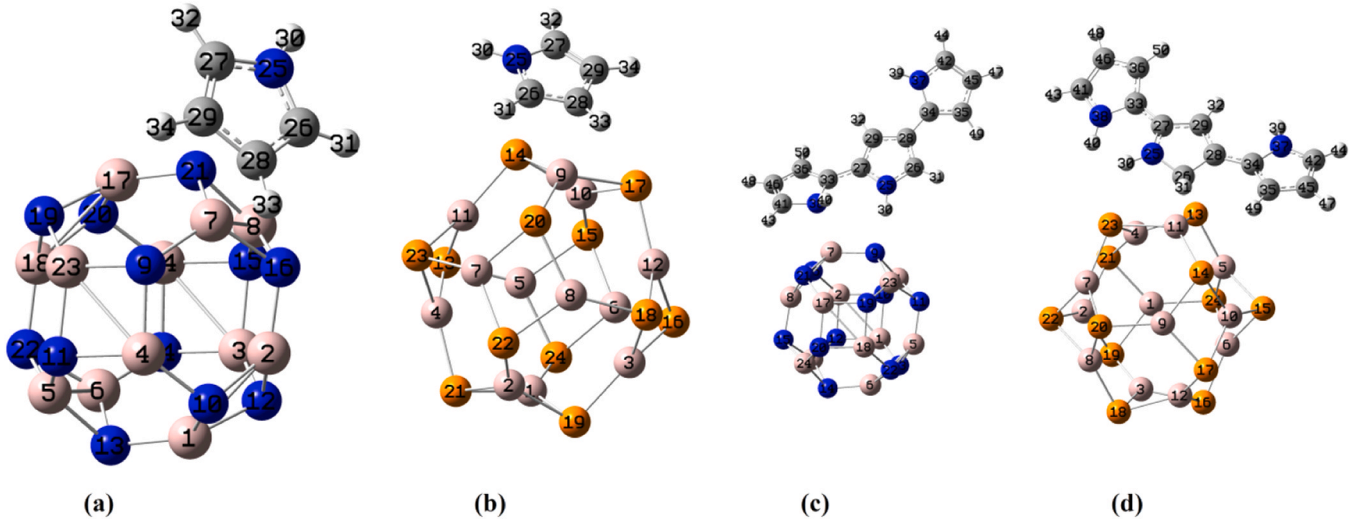

Fig. 2. Optimized geometries of (a) AlN-PYI (b) AlP-PYI (c) AlN-PYII (d) AlP-PYII.

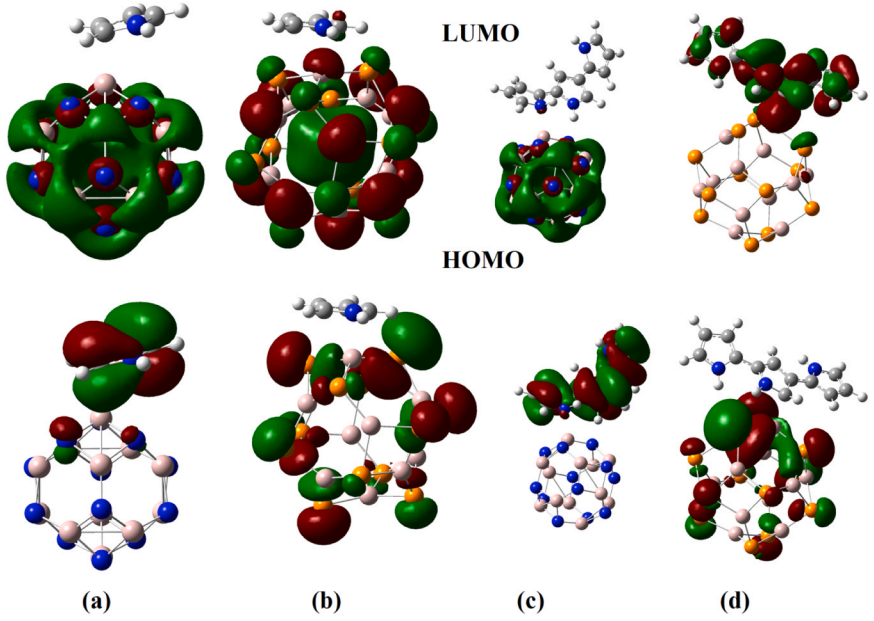

Fig. 3. FMOs of (a) AlN-PYI (b) AlP-PYI (c) AlN-PYII (d) AlP-PYII.

Table 2
Chemical descriptors.

Systems	EH (eV)	EL(eV)	Energy gap (eV)	Hardness (eV)	Chemical Potential (eV)	Electrophilicity index (eV)
PYI	-5.58	-1.27	4.31	2.16	-3.42	2.71
PYII	-4.66	-0.16	4.51	2.25	-2.41	1.29
AlN	-6.47	-2.54	3.93	1.97	-4.51	5.17
AlP	-6.82	-3.43	3.39	1.69	-5.12	7.74
Vacuum						
AlN-PYI	-5.92	-2.06	3.86	1.93	-3.99	4.12
AlP-PYI	-6.23	-2.94	3.29	1.65	-4.59	6.38
AlN-PYII	-4.84	-2.28	2.57	1.28	-3.56	4.94
AlP-PYII	-6.01	-2.83	3.18	1.59	-4.42	6.14
Water						
AlN-PYI	-6.19	-2.22	3.97	1.99	-4.20	4.45
AlP-PYI	-6.15	-2.70	3.45	1.72	-4.42	5.67
AlN-PYII	-4.92	-2.27	2.65	1.33	-3.59	4.87
AlP-PYII	-5.76	-2.68	3.08	1.54	-4.22	5.78

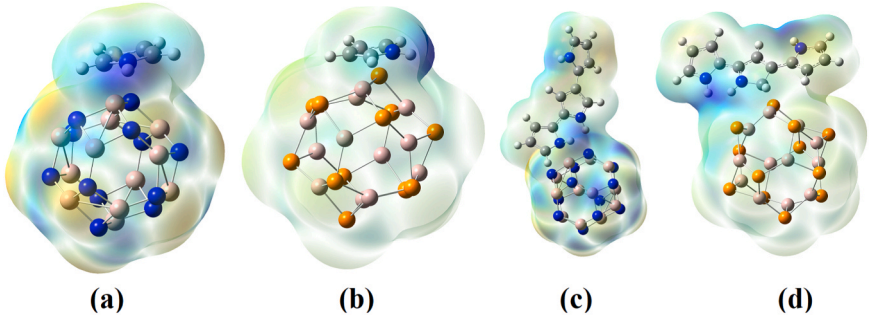

Fig. 4. MEP plots of (a) AlN-PYI (b) AlP-PYI (c) AlN-PYII (d) AlP-PYII.

Table 3
Changes in thermodynamic parameters.

Systems	ΔE (kcal mol^{-1})	ΔH(kcal mol^{-1})	ΔG (kcal mol^{-1})	ΔS (kcal mol^{-1} K^{-1})
Vacuum				
AlN-PYI	-48.26	-47.75	-36.70	-37.057
AlP-PYI	-53.13	-52.73	-41.48	-37.737
AlN-PYII	-122.97	-122.49	-109.82	-42.482
AlP-PYII	-139.80	-189.42	-177.50	-40.000
Water				
AlN-PYI	-74.10	-73.44	-62.84	-35.547
AlP-PYI	-71.93	-71.39	-66.90	-36.115
AlN-PYII	-150.48	-150.95	-134.73	-54.619
AlP-PYII	-161.17	-211.22	-198.05	-44.180

3.2. NBO analysis

Strong hyper conjugative interactions due to lone pairs of N atom in PYI and complexes are: for PYI, N1 to C2-C4 and C3-C5 with energies 34.26 kcal mol^{-1}, while in AlN-PYI, N1 to C3-C5 and C2-C4 with energies 52.19 and 41.25 and in AlP-PYI, N1 to C2-C4 and C3-C5 with energies 51.97 and 48.12 kcal mol^{-1}. For PYII, the interactions are N3 to C10-C11 and C18-C21 with energies, 36.46 and 34.42, N1 to C2-C4 with energy 32.45 kcal mol^{-1}. In AlN-PYII, N14 has interaction energy with C9-C12 and C17-C22 with energies 39.38 kcal mol^{-1}. In AlP-PYII, N13 has energies of 38.75 and 38.37 with C10-C11 and C18-C21, while N14 has an energy of 42.15 kcal mol^{-1} with C9-C12 [78,79]. All these energy values show the interaction after adsorption with nanocages.

The charges (Table S1) obtained from NBO analysis for PYI are −0.56, −0.33 and −0.33 for N1, C4 and C5 while these values become −0.52, −0.53, −0.28 for AlN-PYI and −0.53, −0.50 and −0.28e for AlP-PYII. Other charges also show variations in values due to the adsorption with nanocages. For PYII, the charges of N atoms are −0.55 (N1), −0.56 (N14) while the corresponding values are −0.54 and −0.76e for AlN-PYII. The C atoms have charges −0.06 (C2), 0.10 (C3), −0.14 (C4), 0.09 (C9), −0.30e (C12) and the corresponding charge values are −0.02, 0.07, −0.15, 0.14 and −0.26e for AlN-PYII and −0.46, 0.23, 0.01, 0.07 and −0.25e for AlP-PYII. The changes in charge values suggest the charge transfer between PYI and PYII with nanocages and the process is hence chemisorptions [80].

The Mulliken charges on the drugs following adsorption over the nanoclusters are 0.11 and 0.18e for the PYI complexes and 0.08 and 0.23e for PYII with AlN and AlP cages, respectively [81]. Charge transfer from PYI and PYII to the appropriate nanocluster is indicated by a positive value [82]. Higher charge transfer between adsorbents and adsorbates will lead to the presence of a strong interaction since charge transfer and the presence of a strong interaction are related, and vice versa [83]. In this instance, the quantity of charge transfer causes PYI, PYII, and nanoclusters to interact. Because of the increased charge transfer between PYI and PYII and nanoclusters, this phenomenon confirms the chemisorption.

3.3. Spectral analysis

To analyze the effect of PYs on nanocages, this investigation also used TD-DFT to assist in predicting the UV spectra of all systems. Our goal in this investigation was to examine the PY and produced complexes' UV spectra (Figure S4 and Table S2). PYI's UV–vis shows peak at 182 nm, while in AlN-PYI and AlP-PYI the corresponding peaks are 379 and 426 nm. When nanocages absorb PYI, the power of peak decreased dramatically and shifts to a higher wavelength in all configurations. For PYII there are two peaks in UV at 246 and 281 nm. After adsorption with AlN, these peaks are shifted to 373 and 539 nm while in AlP adsorption, only one peak is observed at 463 nm. In all cases after adsorption with nanocages, there is a reduction in intensity which means the adsorption process is chemisorption [84].

While PYII adsorptions at 246 nm (f=0.9817) and 281 nm (f=0.1634), primarily from mixed H-1→L and H→L+ 1 transitions and a dominant H→L excitation, respectively, the free PYI molecule displays the presence of a strong adsorption at 182 nm with an oscillator strength of 0.1584, dominated by a HOMO→LUMO transition (96%). Strong electronic interaction between the adsorbate and substrate is indicated by noticeable red shifts toward the visible region and a significant decrease in oscillator strength upon adsorption on AlN and AlP surfaces. New absorption bands for AlN-PYI and AlP-PYI emerge at 379 and 426 nm respectively. These bands mostly include deeper occupied orbitals (H-1 or H-2) near the LUMO, indicating a substantial disruption of the frontier molecular orbitals. For PYII complexes, a similar pattern is seen: AlP-PYII displays visible-region absorption at 463 nm with a comparatively greater oscillator intensity (f=0.0284), while AlN displays absorptions at 373 and 539 nm, the latter of which corresponds to a practically pure HOMO→LUMO transition. The suggested sensing and detecting capabilities of the AlN and AlP substrates is supported by these adsorption-induced red shifts and changes in transition character, which offer distinct theoretical spectroscopic fingerprints that may be accessible to practical UV-Vis measurements.

The optimized structures' lack of imaginary frequencies in IR spectrum, are guaranteed vibrational stability, and Raman spectra were used to clarify the SERS augmentation mechanism. The Raman spectra of PYI, PYII and its complexes are given in Figures S5 and S6. The important vibrations modes of AlN are at 902, 427, 351, 188 and 154 and for AlP, the modes are at 518, 490, 454, 437, 301, 216, 198, 112 and 89 cm^{-1}. For PYI, the NH mode is at 3554, which shifts to 3508 cm^{-1} in AlN-PYI and 3500 cm^{-1} in AlP-PYI and the red shift suggest interaction between PYI and nanocage. The CH modes of PYI at 3179 and 3138 appear at 3171 and 3176 cm^{-1} for AlN-PYI and AlP-PYI. The ring modes of PYI are at 1455, 1378, 1130 and 1061 cm^{-1} while in AlN-PYI, these appear at 1463, 1149/1463, 1140 cm^{-1}. In addition peaks are observed at 1522 and 1103 cm^{-1} in AlN-PYI and AlP-PYI which are absent for PYI. Corresponding to the mode at 874 of PYI, modes are found at 899 for AlN-PYI and 849 cm^{-1} for AlP-PYI. In AlN/P-PYI, the nanocage vibrations are found at 422, 353, 185, 145/490, 435, 300, 203, 90 cm^{-1} which agrees with the values of pristine cages.

For PYII, the NH mode is at 3545, which shifts to 3518, 3335 in AlN-PYII and 3515, 3426 cm^{-1} in AlP-PYII and the redshift suggest interaction between PYII and nanocage. In PYII, only one mode corresponding to NH is present while, in AlN/P complexes, the inactive modes of PYII are present due to SERS effect. The CH modes of PYII at 3167 and 3145 appear at 3152, 3000 for AlN-PYII and 3157, 3136, 3030 cm^{-1} in AlP-PYII and here also after adsorption inactive modes of PYII are present in the complexes' spectra. The ring modes of PYII are at 1591, 1499, 1463, 1381, 1340, 1126 cm^{-1} while in AlN-PYII, these appear at 1583, 1561, 1504, 1425, 1330, 1130 cm^{-1} and at 1593, 1509, 1447, 1399, 1362, 1283, 1073 cm^{-1} in AlP-PYII. In addition peaks are observed at 1561, 1362, 867 cm^{-1} in AlN-PYII and 1362, 820, 804 cm^{-1} in AlP-PYII which are absent for PYII. In AlN/P-PYII, the nanocage vibrations are found at 425, 325, 147/530, 310, 205, 95 cm^{-1} which agrees with the values of pristine cages. The presence of inactive modes of PYI and PYII in the complexes after adsorption is due to polarizability changes and SERS effect [85–88].

3.4. Docking analysis

While DFT-based adsorption energies offer a quantitative assessment of binding strength and electrical effects for certain geometries, docking is a configurational and screening approach that finds likely binding orientations, interaction locations, and dominant noncovalent contacts. Particularly for flexible molecules or complex surfaces, adsorption calculations by themselves do not guarantee that the optimized structure corresponds to a physically accessible or likely binding position. Therefore, docking aids in the creation of realistic initial configuration, which DFT then refines and validates. Due to anti-Alzheimer activity of PY's, the protein 1EVE is docked with the title compounds using HDOCK software [89]. The purpose of the HDOCK server is to use a hybrid technique to predict binding complexes between two molecules, such as proteins and nucleic acids. In order to forecast the binding complexes between two molecules, the HDOCK carries out global docking. For docking job, therefore, no information regarding the binding point is required. To increase the accuracy of projected models, the server now provides the ability to produce the binding site residues, should such information be available. When the confidence level is more than 0.7, there is a substantial probability that the two molecules will bind; they would be possible to bind when the score is between 0.5 and 07; and they would be unlikely to bind when the confidence score is below 0.5 [90,91]. The docking scores are −57.35, −183.33, −99.21 for PYI, AlN-PYI, AlP-PYI and −153.80, −216.87, −166.22 for PYII, AlN-PYII, AlP-PYII complexes. In complexes the docking scores are high which indicate the drug delivery carrier effects of nanocages (Table S3). Also the confidence scores are high for complexes in comparison with that of PYI and PYII which support the above argument. The 2D plot of interaction is given in Figure S7.

4. RDG analysis

The RDG isosurface and scatter plots serve to elucidate the nature of interaction between the substrate and analyte, providing visual aid for identification of precise interaction site. The scatter plot highlights the relationship between the RDG function, S(r) and $\rho(r)\text{sign}(\lambda_2)$, where $\rho(r)$ represents the electron density. The sign of λ_2 serves as a pivotal indicator distinguishing the nature of interactions: it is positive for steric interactions and negative for both covalent and noncovalent interactions. Color code for strength of interactions: red/green/ greenish-yellow/blue signifies strong steric repulsion/van der Waals/weak/ strong attraction. The existence of sharp green spikes near low $\rho(r)$ and low S(r) in RDG scatter plots as shown in Figs. 5a,c and 6a,c emphasize

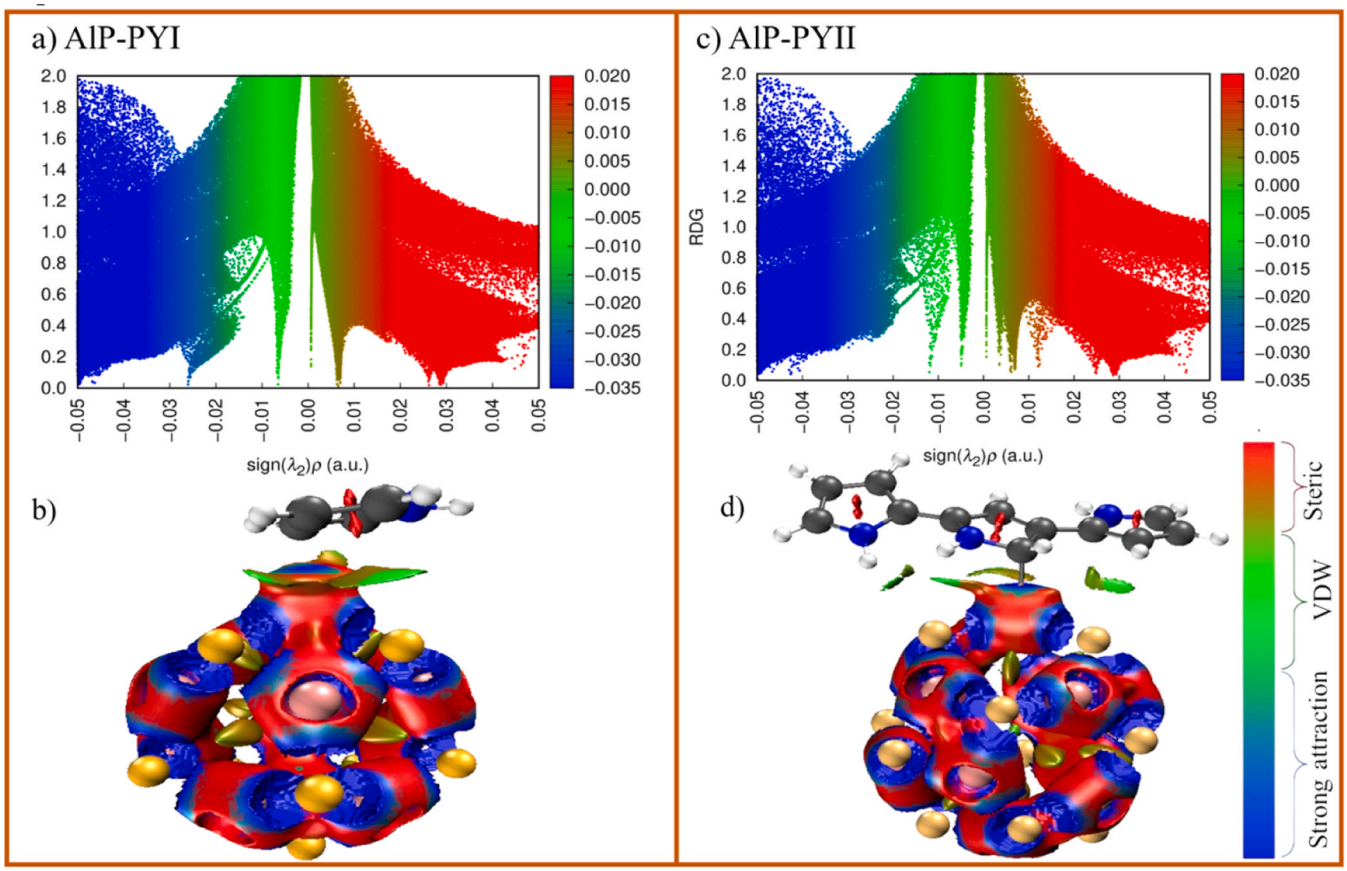

Fig. 5. RDG isosurface (a) (b) and RDG scatter plot (c) (d) for AlP-PYI (AlP-PYII).

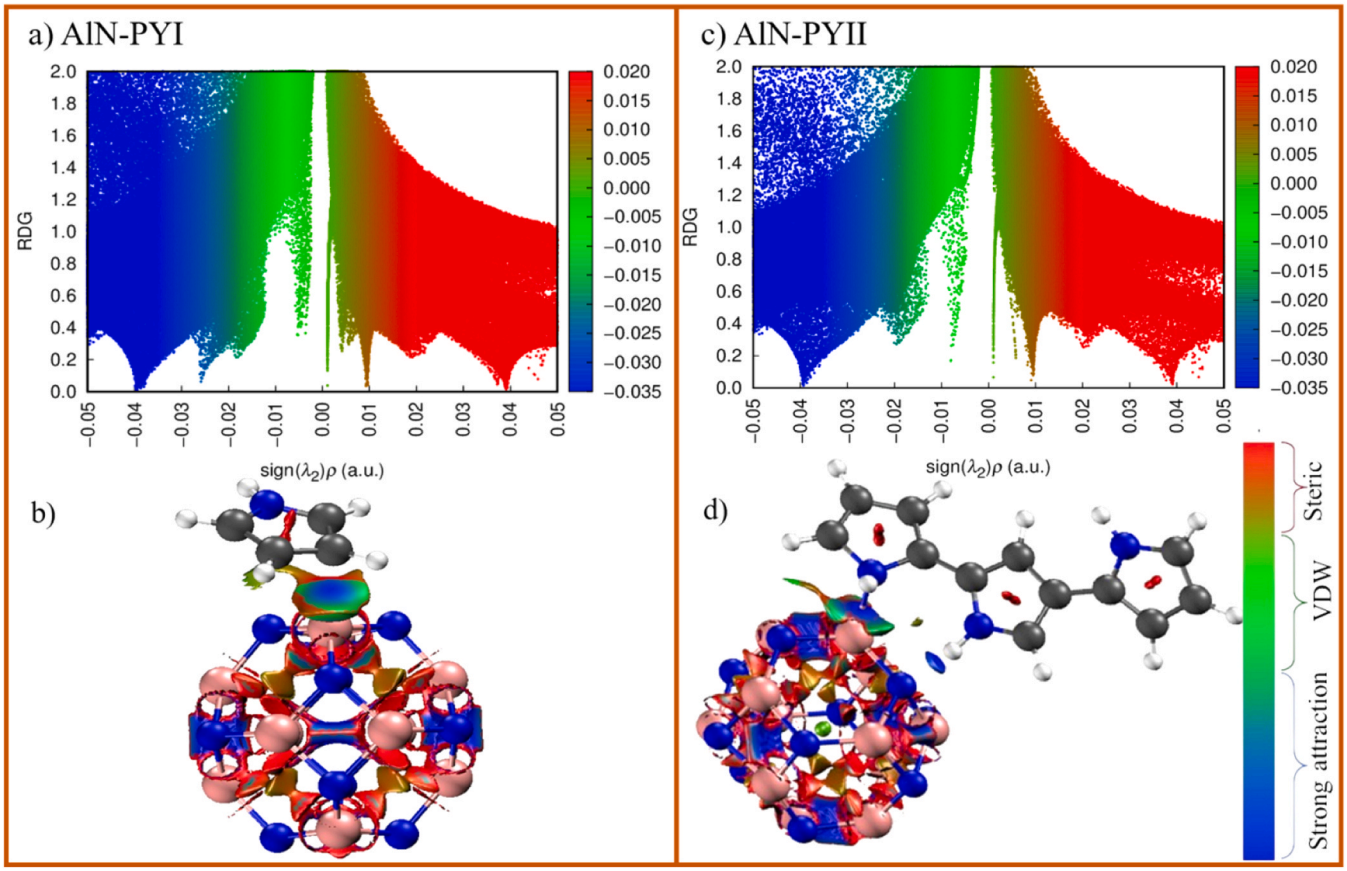

Fig. 6. RDG isosurface (a) (b) and RDG scatter plot (c) (d) for AlN-PYI (AlN-PYII).

the presence of noncovalent interaction. The isosurface plots (Figs. 5b, d and 6b,d) highlights coexistence presence of the strong attraction and VDW kind of interaction between PY's and nanocages, with the dominant influence arising from this strong attraction. For AlP-PYI and AlP-PYII, the carbon atom of pyrrole experiences the predominant attractive force. Furthermore, the presence of a blue disc between the nitrogen atom of the AlN nanocage and the hydrogen of PYII (Fig. 6d) emphasizes the presence of a strong electronic attraction between them [92,93].

4.1. Recovery time

The equation for the conduction electron population is $N = AT^{3/2}$ exp(-Eg/kT) [73]. This method's results often consistent with the experiment's conclusions [94]. When N rises exponentially and Eg declines, an electrical signal is often produced. Nanocages can identify PY by its electrical noise. Additionally, the primary elements of the work function (φ) sensors were examined. A sample's φ is measured before and after PY is adsorbed on nanocages using a Kelvin oscillator. When PY adsorption significantly affects the adsorbent's φ, the gate voltage changes and an electrical signal that aids in PY identification is generated [95]. In sensor-related research, the formula φ =EF is frequently used to express the minimum energy needed to extract one electron from a Fermi level across an indefinite interval. For complexes, the workfunction of PY adsorbed varies from 3.42 to 3.99 and 4.59 for AlN/P-PYI and 2.41–3.56 and 4.42 eV for AlN/P-PYII after adsorption. Changes in the workfunction of the nanocages following PY adsorption imply that the nanocages are not more securely bonded to the electrons. The Richardson Dushman equation explains why the Fermi level varies as a function of workfunction and is connected to changes in the field emission. It asserts that $j = AT^2(\text{exp- } \varphi/kT)$, and φ value are related to the electron current densities [72]. As a result, there is a notable change in the current density released from nanocages, and nanocages can be thought of as a PY adsorption sensor. Strong chemical interactions are not suitable for sensors since a functional sensor required rapid desorption. Technically speaking, adsorption typically results in lengthy recovery times, which are undesirable for sensor applications (Table 4).

The energy gap (Eg) is one of the key factors determining a material's the electrical conductivity and their relationship is expressed as σ = exp (-Eg/2kT) where σ and K are the electrical conductivity and Boltzmann's constant [96]. Thus, the conduction-electron population rises exponentially, and a smaller Eg at a given temperature leads to higher conductivity. Thus, drug adsorption alters the electrical conductivity. Thus, we propose that these nanocages have strong potential as carriers in drug-delivery systems and as components in drug-sensing applications. Recovery time (τ) is a crucial metric in sensor applications and should be determined for both the adsorption and desorption behaviors of the

Table 4
Recovery time (second) for the recovery of PYI & PYII from the nanocage surfaces at 400 K.

Complex	Binding energy (kcal mol^{-1})	Attempt frequency (Hz)			
		3.0×10^{16}	7.5×10^{14}	4.3×10^{10}	1×10^{18}
Vacuum					
AlN-PYI	-25.62	3.32E-03	1.33E-01	2.32E+ 03	9.96E-05
AlP-PYI	-27.19	2.39E-02	9.58E-01	1.67E+ 04	7.18E-04
AlN-PYII	-32.07	1.11E+ 01	4.44E+ 02	7.75E+ 06	3.33E-01
AlP-PYII	-34.03	1.31E+ 02	5.23E+ 03	9.12E+ 07	3.92E+ 00
Water					
AlN-PYI	-33.94	1.17E+ 02	4.67E+ 03	8.14E+ 07	3.50E+ 00
AlP-PYI	-36.17	1.93E+ 03	7.72E+ 04	1.35E+ 09	5.79E+ 01
AlN-PYII	-38.94	6.30E+ 04	2.52E+ 06	4.39E+ 10	1.89E+ 03
AlP-PYII	-39.42	1.15E+ 05	4.61E+ 06	8.04E+ 10	3.46E+ 03

system. The recovery time is defined as $\tau = \upsilon^{-1} \exp(-Eads/kT)$, with T representing the temperature and υ the attempt frequency [96]. According to this equation, higher Eads values result in longer recovery times (τ) because stronger adsorbate-surface interactions hinder desorption, indicating that the system may required extended recovery periods (Table 4). Although long recovery times can restrict their reuse as sensor, the recovery time remains strongly dependent on the attempt frequency and release (desorption) temperature. As shown in the table, the recovery times are within a permissible range, supporting both efficient drug desorption and reusability of the system.

For PYI and PYII adsorbed on AlN and AlP surfaces in vacuum and aqueous media at 400 K, Table 4 shows a considerable reliance of the recovery time on both the binding strength and the estimated attempt frequency. Even for firmly bound PYII species, all complexes show ultrafast recovery (10^{-4} –10^{0} s) at the highest attempt frequency (1×10^{18} Hz), suggesting rapid desorption under highly activated conditions. Recovery time increases systematically when the attempt frequency is lowered to 4.3×10^{10} and 7.5×10^{14} Hz; the effect is more noticeable for PYII than PYI because of their higher binding energies. In vacuum, PYI complexes on AlN and AlP recover in milliseconds to seconds at 3.0×10^{16} Hz, while PYII complexes take seconds to minutes, especially in water. Stronger adsorption energies in solution are compatible with the aqueous environment's dramatic prolongation of recovery across all frequencies; for instance recovery periods increases from ~ 10^{-3} - 10^{2} s in vacuum to ~ 10^{2} - 10^{1} s in water at 3.0×10^{16} Hz. Because of its higher interaction with both PYI and PYII, AlP consistently exhibits longer recovery durations than AlN among the substrates. Overall, the findings show that by varying the attempt frequency, sensor reusability may be adjusted over several orders of magnitude, with moderate frequencies (10^{14} - 10^{16} Hz) providing a workable balance between enough adsorption strength and reasonable recovery durations [97,98].

5. Conclusion

This theoretical study provides detailed insight into the adsorption mechanisms of PYI and PYII on $Al_{12}N_{12}$ and $Al_{12}P_{12}$ nanocages and highlights their strong potential for sensing and biomedical applications. Both pyrrole derivatives bind exothermally to the nanocages and with negative Gibbs free energies, confirming spontaneous chemisorption in vacuum and aqueous environments. Adsorption leads to substantial reorganization of the frontier molecular orbitals, reduced band gaps, increase dipole moments, and enhanced polarizability features that collectively support improved charge transfer and electronic responsiveness of the nanocages upon interaction with the drugs. Spectroscopic analyses reveal notable red shifts in UV-Vis absorption and the appearance of SERS-active Raman modes in the complexes, confirming strong coupling between pyrroles and the cage framework. NBO and RDG analyses identify significant hyperconjugation and mixed noncovalent interactions that contribute to the stability of the adsorbed systems. Docking simulations against the acetylcholinesterase (1EVE) enzyme show markedly enhanced docking and confidence scores for the nanocage drug complexes, indicating improved bioaffinity and the feasibility of these nanocages as drug delivery carriers. Overall, the combined energetic, electronic, spectroscopic, and docking results demonstrated that $Al_{12}N_{12}$ and especially $Al_{12}P_{12}$ nanocages are efficient platforms for pyrrole adsorption, sensing, and targeted photocatalytic technologies.

CRediT authorship contribution statement

Brahmananda Chakraborty: Writing – original draft, Visualization, Investigation, Data curation. **Maria Cristina Gamberini:** Writing – original draft, Visualization, Methodology, Investigation, Data curation. **Mary Dr. Y.Sheena:** Writing – review & editing, Writing – original draft, Visualization, Methodology, Investigation, Data curation. **Unnati Jethawa:** Writing – original draft, Visualization, Methodology, Investigation, Data curation. **S.Al-Otaibi Dr. Jamelah:** Writing – original draft, Visualization, Software, Methodology, Data curation, Conceptualization.

Declaration of Competing Interest

The authors declare that they have no known competing financial interests or personal relationships that could have appeared to influence the work reported in this paper.

Acknowledgments

Princess Nourah Bint Abdulrahman University Researchers Supporting Project number (PNURSP2026R13), Princess Nourah Bint Abdulrahman University, Riyadh, Saudi Arabia.

Appendix A. Supporting information

Supplementary data associated with this article can be found in the online version at doi:10.1016/j.nanoso.2026.101676.

Data availability

Data will be made available on request.

References

[1] P. Zhang, Fabrication of conducting polymer microelectrodes and microstructures for bioelectronics, J. Mater. Chem. C. 9 (2021) 9730–9760, https://doi.org/10.1039/D1TC01618K.
[2] A. Maziz, E. Ozgur, C. Bergaud, L. Uzun, Progress in conducting polymers for biointerfacing and biorecognition applications, Sens. Actuator A Phys. 3 (2021) 100035, https://doi.org/10.1016/j.snr.2021.100035.
[3] F. Xu, M. Zhang, Y. Cui, D. Bao, J. Peng, Y. Gao, D. Lin, H. Geng, Y. Zhu, H. Wang, A novel polymer composite coating with high thermal conductivity and unique anti-corrosion performance, Chem. Eng. J. 439 (2022) 135660, https://doi.org/10.1016/j.cej.2022.135660.
[4] X. Li, X. Chen, Z. Jin, P. Li, D. Xiao, Recent progress in conductive polymers for advanced fiber shaped electrochemical energy storage devices, Mater. Chem. Front. 5 (2021) 1140–1163, https://doi.org/10.1039/D0QM00745E.
[5] H. Sajid, F. Ullah, S. Khan, K. Ayub, M. Arshad, T. Mahmood, Remarkable static and dynamic NLO response of alkali and superalkali doped macrocyclic [hexa-] thiophene complexes: a DFT approach, RSC Adv. 11 (2021) 4118–4128, https://doi.org/10.1039/D0RA08099C.
[6] H. Sajid, F. Ullah, M. Yar, K. Ayub, T. Mahmood, Superhalogen doping: a new and effective approach to design materials with excellent static and dynamic NLO responses, N. J. Chem. 4 (2020) 16358–16369, https://doi.org/10.1039/D0NJ02291H.
[7] H. Ullah, A.G.A. Shah, S. Bilal, K. Ayub, Doping and dedoping processes of polypyrrole: DFT study with hybrid functional, J. Phys. Chem. C. 118 (2014) 17819–17830, https://doi.org/10.1021/jp505626d.
[8] K. Namsheer, C.S. Rout, Conducting polymers: a comprehensive review on recent advances in synthesis, properties, and applications, RSC Adv. 11 (2021) 5659–5697, https://doi.org/10.1039/D0RA07800J.
[9] J. Heck, J. Goding, R.P. Lara, R. Green, The influence of physicochemical properties on the processibility of conducting polymers; a bioelectronics perspective, Acta Biomater. 139 (2022) 259–279, https://doi.org/10.1016/j.actbio.2021.05.052.
[10] L. Du, P. Gao, Y. Meng, Y. Liu, S. Le, C. Yu, Highly efficient removal of Cr(VI) from aqueous solutions by polypyrrole/monodisperse latex spheres, ACS Omega 5 (2020) 6651–6660, https://doi.org/10.1021/acsomega.9b04438.
[11] G. Zhao, X. Huang, Z. Tang, Q. Huang, F. Niu, X. Wang, Polymer-based nanocomposites for heavy metal ions removal from aqueous solution: a review, Polym. Chem. 9 (2018) 3562–3582, https://doi.org/10.1039/C8PY00484F.
[12] E. Vitoratos, S. Sakkopoulose, E. Dalas, P. Malkaj, C. Anestis, DC conductivity and thermal aging of conducting zeolite/polyaniline and zeolite/polypyrrole blends, Curr. Appl. Phys. 7 (2007) 578–581, https://doi.org/10.1016/j.cap.2006.12.001.
[13] G. Wang, A. Morrin, M. Li, N. Liu, X. Luo, Nanomaterial doped conducting polymers for electrochemical sensors and biosensors, J. Mater. Chem. B. 6 (2018) 4173–4190, https://doi.org/10.1039/C8TB00817E.
[14] F.M. Alzahrani, N.S. Alsaiari, K.M. Katubi, A. Amari, F.B. Rebah, M.A. Tahoon, Synthesis of polymer based magnetic nanocomposite for multi pollutants removal from water, Polymers 13 (2021) 1742, https://doi.org/10.3390/polym13111742.
[15] H. Ullah, A.A. Tahir, T.K. Mallick, Structural and electronic properties of oxygen defective and Se-doped p-type BiVO4(001) thin film for the applications of photocatalysis, Appl. Catal. B 224 (2018) 895–903, https://doi.org/10.1016/j.apctb.2017.11.034.

[16] N.A. Mohamed, H. Ullah, J. Safaei, A.F. Ismail, M.F.M. Noh, M.F. Soh, M. A. Ibrahim, N.A. Ludin, M.A.M. Teridi, Efficient photoelectrochemical performance of γ irradiated g-C3N4 and its g-C3N4@BiVO4 heterojunction for solar water splitting, J. Phys. Chem. C. 123 (2019) 9013–9026, https://doi.org/10.1021/acs.jpc.9b00217.
[17] Y. Wang, W. Jia, T. Strout, A. Schempf, H. Zhang, B. Li, J. Cui, Y. Lei, Ammonia gas sensor using polypyrrole-coated TiO2/ZnO nanofibers, Electroanalysis 21 (2009) 1432–1438, https://doi.org/10.1002/elan.200904584.
[18] J.H. Kim, A.K. Sharma, Y.S. Lee, Synthesis of polypyrrole and carbon nano fiber composite for the electrode of electrochemical capacitors, Mater. Lett. 60 (2006) 1697–1701, https://doi.org/10.1016/j.matlet.2005.12.002.
[19] R.G.S. Nair, A.K.N. Nair, S. Sun, Adsorption of gases on B12N12 and Al12N12 nanocages, N. J. Chem. 48 (2024) 8093–8105, https://doi.org/10.1039/D3NJ05703H.
[20] J. Beheshitan, Z. Bagheri, M. Kamfiroozi, A. Ahmadi, A comparative study on the B12N12, Al12N12, B12P12 and Al12P12 fullerene-like cages, J. Mol. Model 18 (2012) 2653–2658, https://doi.org/10.1007/s00894-011-1286-y.
[21] R.G.S. Nair, A.K.N. Nair, S. Sun, Adsorption of drugs on B12N12 and Al12N12 nanocages, RSC Adv. 14 (2024) 31756–31767, https://doi.org/10.1039/D4RA05586A.
[22] M. Boulbazine, I. Djellal, A. Boudjahem, A density functional theory study on the adsorption of β-lapachone anticancer drug onto the MB11N12 (M=Au, Rh and Ru) nanoclusters as a drug delivery, J. Mol. Graph. Model 138 (2025) 109044, https://doi.org/10.1016/j.jmgm.2025.109044.
[23] M. Derdare, N. Cheguib, A. Boudjahem, Effect of metal doping (M=Sc, V, Ti, Fe and Mn) on the sensing performance of the Si12C12 nanocage towards the penicillamine drug molecule: a DFT study, Mol. Phys. 123 (2025) e2349196, https://doi.org/10.1080/00268976.2349196.
[24] N. Cheghib, A. Boudjahem, M. Derdare, R. Boulmokh, B. Bouressace, Study of the chemisorption and sensing performances of the phenytoin molecule onto the Gan (n=3-6), Be12O12, and GaVe11O12 clusters: DFT, DOS, ELF, QTAIM and solvent effects, Prot. Metal. Phys. Chem. Surf. 61 (2025) 77–90, https://doi.org/10.1134/S2070205125700029.
[25] M. Derdare, A. Boudjahem, M. Bouldhazine, Adsorption of the NO_2, N_2O and NH_3 molecules over the C_{20} and MC_{19} (M = Ru, Ir and Au) clusters: a DFT approach, Surf. Interfaces 24 (2021) 101114, https://doi.org/10.1016/j.surfin.2021.101114.
[26] M. Derdare, A. Boudjahem, M. Boulbazine, N. Cheghib, First-principles study on the stability and electronic properties of the Cu- and Rh-doped $B_{12}N_{12}$ nanocages and their sensing performances toward the NO and H2S molecules, Struct. Chem. (2025), https://doi.org/10.1007/s11224-025-02540-1.
[27] A. Soltani, M.R. Taghartphe, V.E. Moghadam, M.B. Javan, F. Heidari, N. Aghaei, P. J. Mahon, Serine adsorption through different functionalities on the $B_{12}N_{12}$ and Pt-$B_{12}N_{12}$ nanocages, Mater. Sci. Eng. C. Mater. Biol. Appl. 92 (2018) 216–227, https://doi.org/10.1016/j.msec.2018.06.048.
[28] M. Derdare, A. Boudjahem, M. Boulbazine, Adsorption and decomposition mechanism of N2O molecule over MC23 (M=Ru, Mn, V, Pd, and Rh) nanoclusters: a comparative DFT investigation, Struct. Chem. 33 (2022) 2043–2062, https://doi.org/10.1007/s11224-022-01984-2.
[29] F. Danhier, O. Feron, V. Preat, To exploit the tumor microenvironment: passive and active tumor targeting of nanocarriers for anticancer delivery, J. Control. Release 148 (2010) 135–146, https://doi.org/10.1016/j.jconrel.2010.08.027.
[30] A. Jana, K.T. Nguyen, X. Li, P. Zhu, N.S. Tan, H. Agren, Y. Zhao, Perylene-derived single component organic nanoparticles with tunable emission; efficient anticancer drug carriers with real time monitoring of drug release, ACS Nano 8 (2014) 5939–5952, https://doi.org/10.1021/nn501073x.
[31] V. Nagarajan, R. Chandiramouli, Investigation of NH3 adsorption behaviour on graphdiynenanosheet and nanotubes: a first principles study, J. Mol. Liq. 249 (2018) 24–32, https://doi.org/10.1016/j.molliq.2017.11.007.
[32] M. Eslami, M. Moradi, R. Moradi, DFT investigation of hydrogen adsorption on the C3N nanotube, Vacuum 133 (2016) 7–12, https://doi.org/10.1016/j.vacuum.2016.08.001.
[33] L. Zhang, J. Xia, Q. Zhao, L. Liu, Z. Zhang, Functional graphene oxide as a nanocarrier for controlled loading and targeted delivery of mixed anticancer drugs, Small 6 (2010) 537–544, https://doi.org/10.1002/smll.200901680.
[34] J. Beheshtian, A.A. Peyghan, Z. Bagheri, M. Kamfiroozi, Interaction of small molecules (NO, H2, N2 and CH4) with BN nanocluster surface, Struct. Chem. 23 (2012) 1567–1572, https://doi.org/10.1007/s11224-012-9970-9.
[35] Z. Bagheri, A.A. Peyghan, DFT study of NO2 adsorption on the AlN nanocones, Comput. Theor. Chem. 1008 (2013) 20–26, https://doi.org/10.1016/j.comptc.2012.12.011.
[36] J. Beheshtian, A.A. Peyghan, M.B. Tabar, Z. Bagheri, DFT study on the functionalization of a BN nanotube with sulfamide, Appl. Surf. Sci. 266 (2013) 182–187, https://doi.org/10.1016/j.apsusc.2012.11.128.
[37] N. Kostoglou, K. Polychronopoulou, C. Rebholz, Thermal and chemical stability of hexagonal boron nitride (h-BN) nanoplatelets, Vacuum 112 (2015) 42–45, https://doi.org/10.1016/j.vacuum.2014.11.009.
[38] D.L. Strout, Structure and stability of boron nitrides: isomers of B12N12, J. Phys. Chem. A 104 (2000) 3364–3366, https://doi.org/10.1021/jp994129a.
[39] R. Wang, D. Zhang, C. Liu, Theoretical prediction of a novel inorganic fullerenelike family of silicon-carbon materials, Chem. Phys. Lett. 411 (2005) 333–338, https://doi.org/10.1016/j.cplett.2005.06.055.
[40] H.-S. Wu, F.-Q. Zhang, X.-H. Xu, C.-J. Zhang, H. Jiao, Geometric and energetic aspects of aluminium nitride cages, J. Phys. Chem. A 107 (2003) 204–209, https://doi.org/10.1021/jp027300i.
[41] S. Gazzari-Jara, D. Cortes-Arrigada, E. Chigo-Anota, S. Miranda-Rojas, Boron-nitrogen fullerenes as electrocatalysts for nitrogen reduction: a computational study of affinity and reaction mechanism, iScience 28 (2025) 112326, https://doi.org/10.1016/j.isci.2025.112326.
[42] G. Garcial-Laiton, F.A.Z. Lopez, E. Shakerzadeh, E. Chigo-Anota, Role of homonuclear B-B/N-N bonds in DNA nucleobases adsorption on boron nitride fullerenes: biosensor and drug transport implications, Comput. Theor. Chem. 1248 (2025) 115188, https://doi.org/10.1016/j.comptc.115188.
[43] Z.M. Shabavi, E. Shakerzadeh, E.C. Anota, Computational analysis of bare and alkali metal-encapsulated Al12N12 nanocages for enhanced removal fluoroquinolone antibiotics from wastewater, J. Mol. Liq. 414 (2024) 126042, https://doi.org/10.1016/j.molliq.2024.126042.
[44] S. Kaushal, M. Kaur, N. Kaur, V. Kumari, P.P. Singh, Heteroatom-doped graphene as sensing materials: a mini review, RSC Adv. 10 (2020) 28608–28629, https://doi.org/10.1039/D0RA04432E.
[45] M.A.A. Ibrahim, M.H.A. Hamda, N.A.M. Moussa, O.H. Abd-Elkader, S.R.M. Saved, M.N. Ahmed, A.M. Awad, T. Shoeib, Aluminium phosphide (Al12P12) nanocage as a potential sensor for volatile organic compounds: a DFT study, RSC Adv. 14 (2024) 13915–13925, https://doi.org/10.1039/D4RA01828a.
[46] A. Bolotsky, D. Butler, C. Dong, K. Gerace, N.R. Glavin, C. Muratore, J.A. Robinson, A. Ebrahimi, Two-dimensional materials in biosensing and healthcare: from in vitro diagnostics to optogenetics and beyond, ACS Nano 13 (2019) 9781–9810, https://doi.org/10.1021/acsnano.9b03632.
[47] Gaussian 16, Revision A.03, M.J. Frisch, G.W. Trucks, H.B. Schlegel, G.E. Scuseria, M.A. Robb, J.R. Cheeseman, G. Scalmani, V. Barone, G.A. Petersson, H. Nakatsuji, X. Li, M. Caricato, A.V. Marenich, J. Bloino, B.G. Janesko, R. Gomperts, B. Mennucci, H.P. Hratchian, J.V. Ortiz, A.F. Izmaylov, J.L. Sonnenberg, D. Williams-Young, F. Ding, F. Lipparini, F. Egidi, J. Goings, B. Peng, A. Petrone, T. Henderson, D. Ranasinghe, V.G. Zakrzewski, J. Gao, N. Rega, G. Zheng, W. Liang, M. Hada, M. Ehara, K. Toyota, R. Fukuda, J. Hasegawa, M. Ishida, T. Nakajima, Y. Honda, O. Kitao, H. Nakai, T. Vreven, K. Throssell, J.A. Montgomery, Jr., J.E. Peralta, F. Ogliaro, M.J. Bearpark, J.J. Heyd, E.N. Brothers, K.N. Kudin, V.N. Staroverov, T.A. Keith, R. Kobayashi, J. Normand, K. Raghavachari, A.P. Rendell, J.C. Burant, S.S. Iyengar, J. Tomasi, M. Cossi, J.M. Millam, M. Klene, C. Adamo, R. Cammi, J.W. Ochterski, R.L. Martin, K. Morokuma, O. Farkas, J.B. Foresman, and D.J. Fox, Gaussian, Inc., Wallingford CT, 2016.
[48] GaussView, Version 6.1, R. Dennington, T.A. Keith, and J.M. Millam, Semichem Inc., Shawnee Mission, KS, 2016
[49] R. Padash, A. Sobhani-Nasab, M. Rahimi-Nasrabadi, M. Mirmotahri, H. Ehrlich, A. S. Rad, M. Peyrvi, Is it possible to use X12Y12 (X=Al, B and Y=N,P) nanocages for drug delivery systems? A DFT study on the adsorption properties of 4-aminopyridine drug, Appl. Phys. A 124 (2018) 582, https://doi.org/10.1007/s00339-018-1965-y.
[50] N. Kosar, M. Amjad, M.Z. Ahmed, M. Raja, T. Mahmood, Quantum chemical exploration of B2C2N2 nanosheet as anticancer drug delivery substrate, Comput. Theor. Chem. 1241 (2024) 114847, https://doi.org/10.1016/j.comptc.2024.114847.
[51] J. Cahi, M. Head-Gorden, Long-range corrected hybrid density functionals with dampled atom-atom dispersion corrections, Phys. Chem. Chem. Phys. 10 (2008) 6615–6620, https://doi.org/10.1039/B810189B.
[52] L. Goerigk, S. Grimme, Efficient and accurate double-hybrid-meta-GGA density functional- evaluation with the extended GMTKN30 database for general main group thermochemistry, kinetics, and noncovalent interactions, J. Chem. Theory Comput. 7 (2011) 291–300, https://doi.org/10.1021/ct100466k.
[53] N. Mardirossian, M. Head-Gordon, Thirty years of density functional theory in computational chemistry: an overview and extensive assessment of 200 density functionals, Mol. Phys. 115 (2017) 2315–2372, https://doi.org/10.1080/00268976.2017.1333644.
[54] M. Dolg, U. Wedig, H. Stoll, H. Preuss, Energy-adjusted ab initio pseudopotentials for the first row transition elements, J. Chem. Phys. 86 (1987) 866–872, https://doi.org/10.1063/1.452288.
[55] C. Sosa, J. Andzelm, B.C. Elkin, E. Wimmer, K.D. Dobbs, D.A. Dixon, A local density functional study of the structure and vibrational frequencies of molecular transition-metal compounds, J. Phys. Chem. 96 (1992) 6630–6636, https://doi.org/10.1021/j100195a022.
[56] A.S. Rad, Study on the surface interaction of furn with X12Y12 (X=B, Al and Y=N, P) semiconductors: DFT calculations, Heteroat. Chem. 27 (2016) 316–322, https://doi.org/10.1002/hc.21342.
[57] A.S. Rad, K. Ayub, Coordination of nickel atoms with Al12X12 (X=N,P) nanocages enhances H2 adsorption: a surface study by DFT, Vacuum 133 (2016) 70–80, https://doi.org/10.1016/j.vacuum.2016.08.017.
[58] H. Ullah, K. Ayub, Z. Ullah, M. Hanif, R. Nawas, A.A. Shah, S. Bilal, Theoretical insight of polypyrrole ammonia gas sensor, Synth. Met. 172 (2013) 14–20, https://doi.org/10.1016/j.synthmet.2013.03.021.
[59] J.G. Brandenburg, M. Alessio, B. Civalleri, M.F. Peintinger, T. Bredow, S. Grimme, Geometrical correction for the inter- and intramolecular basis set superposition error in periodic density functional theory calculations, J. Phys. Chem. A 117 (2013) 9282–9292, https://doi.org/10.1021/jp406658y.
[60] ⟨https://wwwtc.thch.uni-bonn.de/⟩.
[61] L. Kruse, L. Goerigk, S. Grimme, Why the standard B3LYP/6–31 G* model chemistry should not be used in DFT calculations of molecular thermochemistry: understanding and correcting the problem, J. Org. Chem. 77 (2012) 10824–10834, https://doi.org/10.1021/jo302156p.
[62] H.R.A. El-Mageed, F.M. Mustafa, K.M.K. Abdel-Latif, The ability of gold nanoclusters as a new nanocarrier for D-penicillamine anticancer drug: a computational chemistry study, Struct. Chem. 31 (2020) 781–793, https://doi.org/10.1007/s11224-019-01462-2.

[63] Z. Ullah, H.J. Kim, Y.S. Mary, N. Belboukhari, K. Sekkoum, A. Kraimi, X. Zhang, H. W. Kim, Unlocking the potential of ovalene: a dual-purpose sensor and drug enhancer, J. Mol. Liq. 377 (2023) 121540, https://doi.org/10.1016/j.molliq.2023.121540.
[64] Z. Ullah, H.J. Kim, Y.S. Mary, H.W. Kwon, Insights into caffeine adsorption on the surface of corannulene: a sensor study, J. Mol. Liq. 368 (2022) 120592, https://doi.org/10.1016/j.molliq.2022.120592.
[65] T. Lu, F. Chen, Multiwfn: a multifunctional wavefunction analyzer, J. Comput. Chem. 33 (2012) 580–592, https://doi.org/10.1002/jcc.22885.
[66] W. Humphrey, A. Dalke, K. Schulten, VMD: visual molecular dynamics, J. Mol. Graph 14 (1996) 33–38, https://doi.org/10.1016/0263-7855(96)00018-5.
[67] J.S. Al-Otaibi, Y.S. Mary, Y.S. Mary, R. Thomas, Evidence of cluster formation of pyrrole with mixed silver metal clusters, Agx-My (x=4,5, y=2/1) and M=Au/Ni/Cu) using DFT/SERS analysis, Comp. Theor. Chem. 1208 (2022) 113569, https://doi.org/10.1016/j.comptc.2021.113569.
[68] Y.S. Priya, K.R. Rao, P.V. Chalapathi, A. Veeraiah, K.E. Srikanth, Y.S. Mary, R. Thomas, Intricate spectroscopic profiling, light harvesting studies and other quantum mechanical properties of 3-phenyl-5-isooxazolone using experimental and computational strategies, J. Mol. Struct. 1203 (2020) 127461, https://doi.org/10.1016/j.molstruc.2019.127461.
[69] J.S. Al-Otaibi, Y.S. Mary, Y.S. Mary, S. Kaya, S. Erkan, Spectral analysis and DFT investigation of some benzopyran analogues and their self assemblies with graphene, J. Mol. Liq. 317 (2020) 113924, https://doi.org/10.1016/j.molliq.2020.113924HOMO.
[70] J.S. Al-Otaibi, Y.S. Mary, Y.S. Mary, Z. Ullah, R. Yadav, N. Gupta, D.G. Churchill, Adsorption properties of dacarbazine with graphene/fullerene/metal nanocages-reactivity, spectroscopic and SERS analysis, Spectrochim. Acta 268 (2022) 120677, https://doi.org/10.1016/j.saa.2021.120677.
[71] J.S. Al-Otaibi, Y.S. Mary, Y.S. Mary, Z. Ullah, H.W. Kwon, Adsorption behaviour and solvent effects of an adamantine-triazole derivative on metal clusters – DFT simulation studies, J. Mol. Liq. 345 (2022) 118242, https://doi.org/10.1016/j.molliq.2021.118242.
[72] J.S. Al-Otaibi, Y.S. Mary, Y.S. Mary, N. Acharjee, Z. Ullah, DFT, solvation effects, reactivity and SERS analysis on structural, optical, and vibrational properties of a biomolecule of pyrimidine derivative adsorbed on metal clusters of Ag./Au/Cu, J. Indian. Chem. Soc. 99 (2022) 100753, https://doi.org/10.1016/j.jics.2022.100753.
[73] Z. Ullah, H.J. Kim, Y.S. Mary, X. Zhan, H.W. Kim, Adsorption of pyrimidin-2-amine (PA) on graphene quantum dots (GQDs): non-covalent interaction study, J. Mol. Liq. 368 (2022) 120654, https://doi.org/10.1016/j.molliq.2022.120654.
[74] Z. Ullah, H.J. Kim, S. Jang, Y.S. Mary, H.W. Kwon, DFT study of 6-amino-3-(1-hydroxyethyl)pyridine-2,4-diol (AHP) adsorption on coronene, J. Mol. Liq. 360 (2022) 119436, https://doi.org/10.1016/j.molliq.2022.119436.
[75] J.-J. Zheng, Q.-Z. Li, Z. Wang, X. Wang, Y. Zhao, X. Gao, Computer-aided nanodrug discovery: recent progress and future prospects, Chem. Soc. Rev. 53 (2024) 9059–9132, https://doi.org/10.1039/D3CS00575E.
[76] K. Basu, V.S. Chelagamsetty, V.A. Ruiz-Avila, T. Li, Machine learning prediction of protein adsorption on drug-delivering nanoparticles: a literature survey and need for future development, Pharm. Res. (2005), https://doi.org/10.1007/s11095-025-03981-6.
[77] N. Jahan, A. Alam, M. Rahman, M. Honque, H. Ahmad, Mesoporous Fe3O4/SiO2/poly(2-carboxyehtylacrylate) composite polymer particles for pH-responsive loading and targeted release of bioactive molecules, RSC Adv. 14 (2024) 23560–23573, https://doi.org/10.1039/d4ra03160a.
[78] Y.S. Mary, H.T. Varghese, C.Y. Panicker, T. Thiesmann, A.A. Al-Saadi, S. A. Popoola, C. Van Alsenoy, Y.A. Jasem, Molecular conformational analysis, vibrational spectra, NBO, NLO, HOMO-LUMO and molecular docking studies of ethyl 3-ϵ-(anthracen-9-yl)prop-2-enoate based on density functional theory calculations, Spectrochim. Acta 150 (2015) 533–542, https://doi.org/10.1016/j.saa.2015.05.092.
[79] J.A. War, K. Jalaja, Y.S. Mary, C.Y. Panicker, S. Armakovic, S.J. Armakovic, S. K. Srivastava, C. Van Alsenoy, Spectroscopic characterization of 1-[3-(1H-imidazol-1-yl)propyl]-3-phenylthiourea and assessment of reactive and optoelectronic properties employing DFT calculations and molecular dynamics simulations, J. Mol. Struct. 1129 (2017) 72–85, https://doi.org/10.1016/j.molstruc.2016.09.063.
[80] F. Sattar, Z. Wang, X. Zhou, Z. Ullah, Battling hazardous gas molecules with kekulene surfaces: a computational study, J. Mol. Liq. 407 (2024) 125099, https://doi.org/10.1016/j.molliq.2024.125099.
[81] S. Vadalkar, D. Chodvadiya, N.N. Som, K.N. Vyas, P.K. Jha, B. Chakraborty, An ab-initio study of the C18 nanocluster for hazardous gas sensor application, ChemistrySelect 7 (2022) e202103874, https://doi.org/10.1002/slct.202103874.
[82] S.K. Jana, N.N. Som, P.K. Jha, Theoretical appraisements on the interaction behaviour of amphetamine, ketamine and mercatpopurine drug molecules over C24 fullerene: a combined dispersion corrected DFT and MD simulation study, J. Mol. Liq. 383 (2023) 122084, https://doi.org/10.1016/j.molliq.2023.122084.
[83] A.S. Rad, First principles study of Al-doped graphene as nansostructure adsorbent for NO2 and N2O: DFT calculations, Appl. Surf. Sci. 357 (2015) 1217–1224, https://doi.org/10.1016/j.apsusc.2015.09.168.
[84] P. Vennila, J.S. Al-Otaibi, G. Venkatesh, Y.S. Mary, V. Raj, N. Acharjee, P. Tamilselvi, Structural, spectral, molecular docking, and molecular dynamics simulations of phenylthiophene-2-carboxylate compounds as potential anticancer agents, Poly. Arom. Compd. 44 (2024) 238–260, https://doi.org/10.1080/10406638.2023.2172052.
[85] A.H. Almuqrin, J.S. Al-Otaibi, Y.S. Mary, Y.S. Mary, R. Thomas, Structural study of letrozole and metronidazole and formation of self assembly with graphene and fullerene with the enhancement of physical, chemical and biological activities, J. Biomol. Struct. Dyn. 39 (2021) 5509–5515, https://doi.org/10.1080/07391102.2020.1790420.
[86] Y.S. Mary, K. Raju, T.E. Bolelli, I. Yildiz, H.I.S. Nogueira, C.M. Granadeiro, C. Van Alsenoy, FT-IR, FT-Raman, surface enhanced Raman scattering and computational study of 2-(p-fluorophenyl)-6-nitrobenzoxazole, J. Mol. Struct. 1012 (2012) 22–30, https://doi.org/10.1016/j.molstruc.2011.12.042.
[87] J.S. Al-Otaibi, Y.S. Mary, Y.S. Mary, G. Serdaroglu, Adsorption of adipic acid in Al/B-N/P nanocages: DFT investigations, J. Mol. Model 27 (2021) 113, https://doi.org/10.1007/s00894-021-04742-z.
[88] J.S. Al-Otaibi, Y.S. Mary, Y.S. Mary, M. Kratky, J. Vinsova, M.C. Gamberini, Concentration dependent SERS profile of p-tolyl 2-acetamido-3-(4-fluorophenl) propanoate (AFP) in silver colloidal nanohydrosols: experimental and DFT investigations, J. Mol. Struct. 1290 (2023) 135998, https://doi.org/10.1016/j.molstruc.2023.135998.
[89] G. Kryger, I. Simon, J.L. Sussman, Structure of acetylcholinesterase complexed with E2020 (Aricept): implications for the design of new anti-alzheimer drugs, Structure 7 (1999) 297–307, https://doi.org/10.1016/s-969-2126(99)80040-8.
[90] Y. Yan, H. Tao, J. He, S.-Y. Huang, The HDOCK server for integrated protein-protein docking, Nature (2020), https://doi.org/10.1038/s41596-020-0312-x.
[91] ⟨http://hdock.phys.hust.edu.cn/⟩.
[92] Z. Ullah, F. Sattar, H.J. Kim, S. Jang, Y.S. Mary, X. Zhan, H.W. Kwon, Computational study of toxic gas removal, J. Mol. Liq. 365 (2022) 120213, https://doi.org/10.1016/j.molliq.2022.120213.
[93] Z. Ullah, F. Sattar, H.J. Kim, S. Jang, Y.S. Mary, X. Zhan, H.W. Kwon, Computational study of Pd-Cd bimetallic crystals: spectroscopic properties, hirshfeld surface analysis, non-covalent interaction and sensor activity, J. Mol. Liq. 365 (2022) 120111, https://doi.org/10.1016/j.molliq.2022.120111.
[94] A. Abbasi, J.J. Sardroodi, Exploration of sensing of nitrogen dioxide and ozone molecules using novel TiO2/stanene heterostructures employing DFT calculations, Appl. Surf. Sci. 442 (2018) 368–381, https://doi.org/10.1016/j.apsusc.2018.02.183.
[95] J.S. Al-Otaibi, Y.S. Mary, Y.S. Mary, N. Acharjee, D.G. Churchill, Theoretical study of glycoluril by highly symmetrical magnesium oxide Mg12O12 nanostructure: adsorption, detection, SERS enhancement and electrical conductivity study, J. Mol. Model 28 (2022) 332, https://doi.org/10.1007/s00894-05332-3.
[96] M.D. Ganji, H. Ko, S. Jamehbozorgi, M. Tajbakhsh, S. Tanreh, R.P. Nejad, M. Sepahvand, M. Rezvani, Unravelling performance of honeycomb structures as drug delivery systems for the isoniazid drug using DFT-D3 correction dispersion and molecular dynamics simulations, Phys. Chem. Chem. Phys. 26 (2024) 14018, https://doi.org/10.1039/d3cp05457h.
[97] M. Derdare, A. Boudjahem, Adsorption of the guanine molecule over the pristine, nb-, and Au-doped boron nitride nanosheets: a DFT study, Struct. Chem. 32 (2021) 2159–2173, https://doi.org/10.1007/s11224-021-01785-z.
[98] A. Boudjahem, M. Derdare, N. Cheghib, Adsorption and sensing performances of the greenhouse gas molecules (HCOH, CO, H2S, CH4 and SO2) by the pristine and metal(M)-doped germanene (M=Rh, Cr and Mo) monolayers: a DFT investigation, Struct. Chem. (2025), https://doi.org/10.1007/s11224-025-02612-5.